Oxygen-ion arrangements and concerted motion in β-La$_2$Mo$_2$O$_9$

C. J. Hou,[1] Y. D. Li,[1,2] P. J. Wang,[1] C. S. Liu,[1,*] X. P. Wang,[1] Q. F. Fang,[1] and D. Y. Sun[3]

[1]*Key Laboratory of Materials Physics, Institute of Solid State Physics, Chinese Academy of Sciences, P.O. Box 1129, Hefei 230031,*
People's Republic of China

[2]*Department of Physics, Anhui University, Hefei 230039, People's Republic of China*

[3]*Department of Physics, East China Normal University, Shanghai 200062, People's Republic of China*

(Received 5 April 2007; revised manuscript received 23 May 2007; published 10 July 2007)

We have performed *ab initio* molecular dynamics simulations coupled to a simulated annealing procedure and the nudged elastic band method to study the arrangements and diffusion of O ions in β-La$_2$Mo$_2$O$_9$. It is found that the occupancies of three crystallographic distinct O sites O(1), O(2), and O(3) are 100%, 91.7%, and 25%, respectively, consistent with experiments. Each Mo cation is surrounded by four or five O ions, forming MoO$_4$ tetrahedra or MoO$_5$ hexahedra. The analysis of Mo-O(1) bond length demonstrates the split of O(1) sites into two groups. The O ions move in a cooperative fashion. Two diffusion channels are found to be responsible for the high conductivity, one involves the migration of O(2) with low barrier energy and short migration length assisted by O(3), and another is the migration of O(3) with large barrier energy and long migration length assisted by O(1) and O(2). The thermally activated and concerted motions of three different kinds of O ions instead of the single-particle jump indicate that the diffusion or relaxation behaviors in β-La$_2$Mo$_2$O$_9$ could be understood using the combined model of Arrhenius law and Vogel-Tammna-Fulcher equation.

I. INTRODUCTION

The atomic processes involved in solid-state diffusion are of broad scientific and technological interest. As a result, efforts have been made over the years to determine the basic mechanisms of atom diffusion in a wide variety of systems. However, in the important case of fast oxide ion conductors, the detailed mechanisms of ion diffusion have proved extremely elusive.[1–7] A complete knowledge of the atomic mechanism of O ion diffusion is a fundamental issue to find other materials with high conductivity. Recently, Lacorre *et al.*[1,8–10] have reported another kind of oxygen-ion conductor, lanthanum molybdate La$_2$Mo$_2$O$_9$, which exhibits good ionic conductivity as high as 0.06 S/cm at 800 °C. They found that it undergoes a reversible phase transition from a low-temperature form α-La$_2$Mo$_2$O$_9$ to a high-temperature form β-La$_2$Mo$_2$O$_9$ at 580 °C. The high-temperature form β-La$_2$Mo$_2$O$_9$ has a cubic structure and $P2_13$ space group, which is determined using x-ray and neutron diffraction data plus the derivation from the structure of β-SnWO$_4$ based on the so-called lone pair substitution concept. The key feature of β-La$_2$Mo$_2$O$_9$ is three crystallographic distinct O ion sites with different occupancies, resulting in a high concentration of intrinsic O vacancies. O(1) sites (representing 22% of the oxide ions) are fully occupied. Two of three crystallographic O sites, O(2) and O(3), representing about 78% of all oxide ions in β-La$_2$Mo$_2$O$_9$ (53% and 25%, respectively), are partially (87% and 29%, respectively) occupied. The high concentration of intrinsic O vacancies provides enough paths for O ion diffusion and is responsible for the high anionic conductivity of β-La$_2$Mo$_2$O$_9$. The crystal structure of low-temperature phase α-La$_2$Mo$_2$O$_9$ remains unknown up to now. It most probably originates from an ordering oxide ions and vacancies and is a $2\times3\times4$ superstructure related to the high-temperature phase. The various NMR experiments carried out by Emery *et al.*[11] on α-La$_2$Mo$_2$O$_9$ give evidence of

four broad, partly overlapping types of distributed contributions in the ^{17}O spectra, which were attributed to the different O ions sites of O(1), O(2), and O(3) of the high-temperature phase. Note that the power diffraction data of La$_2$Mo$_2$O$_9$ allow us to locate the cationic positions but do not allow one to be firmly conclusive about the exact O ion locations. Such a difficulty as locating conducting ions is rather common in ionic conductors due to the strong *delocalization* of such atoms. This is evidenced by the large thermal factors for O ions.

We have recently performed the mechanical and dielectric relaxation studies on the mechanism of O ion diffusion in La$_2$Mo$_2$O$_9$.[4] We observed in the mechanical relaxation measurement a prominent relaxation peak around 400 K at a measurement frequency of 1 Hz, which is actually composed of two subpeaks, P_1 and P_2. As for the dielectric experiment, only one relaxation peak P_d is observed above 600 K when the measured frequency is greater than 500 Hz. The two mechanical relaxation subpeaks and the dielectric relaxation peak follow the Arrhenius law in the relationship between the frequency and the peak temperature, yielding the activation energies of P_1, P_2, and P_d peaks, 0.9, 1.1, and 0.99 eV, respectively. We suggested that the P_2 peak with much larger relaxation strength may be associated with the short-distance diffusion between O(1) and O(3), while the P_1 peak may be related to the diffusion process between O(1) and O(2) via the vacancy mechanism. Therefore, we proposed that a path of long-distance diffusion of O ions may be the jumps of O ions or vacancies from the O(1) site to O(2), then to O(3), and again to O(1): O(1)↔O(2)↔O(3)↔O(1). However, the peak height or relaxation strength hardly changes with temperature. In addition, the conductivity versus temperature curves can be modeled by the Vogel-Tammna-Fulcher (VTF) equation.[2,3,5] These could not be understood by the conventional single-vacancy jump mechanism. In order to understand the relaxation processes originating from the short-

range diffusion of O ions via vacancies, further theoretical analysis on the crystal structure is necessary. It is most usual to assume that the mobile particles in the solid move independently and randomly and the transport properties are understood using the concept of single-particle diffusion. It may be unrealistic in $La_2Mo_2O_9$ because of the high concentration of mobile oxygen ions.

The structural aspects of the O ion or O vacancy distributions on the available crystallographic sites and how these relate to the mechanism of ionic conductivity are of intense interest and important for understanding high oxide ion conductivity of β-$La_2Mo_2O_9$. Because O(1) sites are fully occupied and O(2) and O(3) are partially occupied, it is directly suggested that O ions in O(2) and O(3) sites but in O(1) sites are mobile charge carriers. Is this argument correct? Do the mobile ions move independently or in a cooperative fashion? In this work, we use *ab initio* molecular dynamics (MD) simulations coupled to a simulated annealing procedure to study the structure properties of β-$La_2Mo_2O_9$ and the nudged elastic band (NEB) method to investigate diffusion properties of O ions. The paper is organized as follows: in Sec. II, we describe the method of our simulations; the results of our simulations and the corresponding discussion are reported in Sec. III; a short summary is given in Sec. IV.

II. COMPUTATIONAL METHODS

Our *ab initio* MD simulations were performed within the framework of the density-function theory, with the local density approximation to the exchange-correlation energy, and the valence electron-ion interaction was modeled by the projector augmented-wave potential,[12,13] as implemented in the Vienna ab initio simulation package.[14] The configurations $[He]2s^22p^4$ for O, $[Kr]4d^55s^1$ for Mo, and $[Kr4d]5s^25p^65d^16s^2$ for La were treated as valence electrons. The atoms of system were put in a simple cubic box with periodical boundary condition. A $2\times2\times2$ k-point mesh was generated using the Monkhorst-Pack scheme.[15] The electronic wave functions were expanded in the plane wave basis with an energy cutoff of 650 eV. The Verlet algorithm was used to integrate Newton's equations of motion and the time step of ion motion was 2 fs. To predict structure of the crystal, an available method is to use simulated annealing, where molecular dynamics is used to simulate heating and cooling of a structure from a guessed structure. Though the method of simulated annealing has proved to be one of the most successful methods for finding the global minima, it is usually considered to be too time consuming in combination with first principles methods especially for the system including transition metals. So the simulation system is small. In order to conciliate this disadvantage with the small system, our calculations began with different initial structures. If the cooling rate is slow enough, the resultant structures do not in nature depend on the initial input structures and thus correspond to the global minima.

In our present work, the input structures of β phase were based on the experimental data given in Table 2 of Ref. 8. Based on the results of the x-ray diffraction pattern of β-$La_2Mo_2O_9$ and the structural relationship with β-$SnWO_4$,

β-$La_2Mo_2O_9$ has the same space group $P2_13$ and the identical cationic positions as β-$SnWO_4$. That is, β-$La_2Mo_2O_9$ can be viewed as β-$SnWO_4$ at where Sn is replaced by La and W by Mo, and an extra O atom is necessary to fulfill the oxidation state because La is trivalent. At 900 K, cubic cell parameter $a=7.2014$ Å. For our 26-atom supercell, three starting input models contained 4 La and 4 Mo atoms and 18 O atoms distributed in 28 available crystallographic sites of the $P2_13$ space group: in model A 18 O atoms locate on 4 O(1) and 12 O(2) sites and 2 O(3) sites, that is, both O(1) and O(2) sites are fully occupied but O(3) sites are 16.7% occupied; in model B 18 O atoms locate on 4 O(1) sites and 7 O(2) and 7 O(3) sites, i.e., O(1) are fully occupied but both O(2) and O(3) sites are 50% occupied; in model C 18 O atoms locate on 2 O(1) and 4 O(2) sites and 12 O(3) sites, i.e., both O(1) and O(2) sites are partially (50% and 33.3%, respectively) occupied but O(3) sites are fully occupied. In other words, among the three input models at least two of three crystallographic distinct O ion sites have different occupancies. We firstly heated up the starting model A or B or C system from 0 to 1500 K within 20 ps to get its liquid. At this temperature, the systems were equilibrated for 20, 24, 28, and 32 ps, which means that from each starting model we could obtain 4 initial configurations at 1500 K for the subsequent cooling runs, resulting in 12 initial configurations at 1500 K from three starting models. In a word, 12 initial configurations of all cooling runs are obtained from different starting models with different occupancy possibilities of different O sites or from different equilibration times so different in local structures of O ions. Then the systems were gradually cooled down to 900 K with a sequentially cooling model, which means that after a period of temperature drop it experienced a relaxation process with 10 000 steps. Then the systems were directly quenched from 900 to 0 K to avoid the structural transition from β phase to α phase at 853 K and to reach their local or inherent structures (i.e., remove the thermal motions).[16,17] These 12 inherent structural configurations were saved for analyzing the microstructures on the distribution of O ions and as the input structures for studying the diffusion properties of O ions by the NEB method.[18] The NEB method is a reliable way to find the minimum-energy paths, when the initial and final states of a process are known. An interpolated chain of configurations (images) between the initial and final positions is connected by springs and relaxed simultaneously to the minimum-energy path. With the climbing image scheme, the highest-energy image climbs uphill to the saddle point. Transition states isolated with NEB are further optimized by using a conjugate gradient algorithm in order to minimize the forces on each of the movable atoms. During all the MD calculations, La and Mo atoms are fixed, since the power diffraction data of $La_2Mo_2O_9$ allow us to locate their positions exactly.

III. RESULTS AND DISCUSSION

To characterize the dynamic properties and the structural changes during the simulated annealing process, we have calculated the time-dependent mean-square displacement (MSD) and the root-mean-square fluctuation of Mo-O bond length at various temperatures,[19,20]
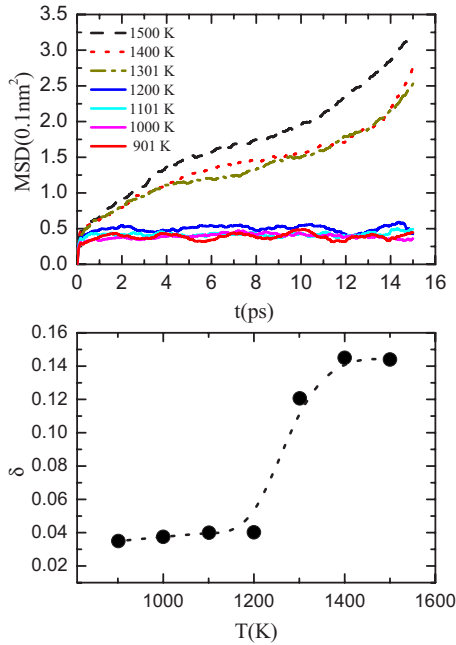
FIG. 1. (Color online) Upper panel, the mean-square atomic displacements (MSDs) of O ions versus time at seven different temperatures; lower panel, the root-mean-square Mo-O bond-length fluctuations δ as a function of temperature. The dotted line is a guide to the eyes.

$$\delta = \frac{1}{18}\sum_{i=1}^{18}\frac{(\langle R_{ij}^2\rangle - \langle R_{ij}\rangle^2)^{1/2}}{\langle R_{ij}\rangle}, \qquad (1)$$

where $\langle\;\rangle$ is the average over the entire trajectory, and R_{ij} is the distance between the O ion i and its neighboring Mo cation j. Figure 1 shows the time evolution of MSD for O ions at seven different temperatures in the upper panel and the root-mean-square fluctuation δ of Mo-O bond length versus temperature in the lower panel. The MSD shows a saturation for the large t at temperature $\leqslant 1200$ K. On the other hand, liquidlike behavior at high temperature is evident from the rapid increase behavior of MSD with time. With the decrease of temperature, there is a sudden drop in δ around 1300–1200 K. This step-function-like behavior of δ and the appearance of a wide gap in the MSD-t curves in the temperature range 1300–1200 K indicate that a liquid-solid phase transition takes place in our simulated system, that is, the simulated system is crystallized. The energy difference between the highest- and lowest-energy configurations is smaller than 0.004 eV, indicating that the identical structure is obtained from different starting configurations. Therefore, the 12 final configurations (see Fig. 2) quenched from 900 K represent the geometry of β-La$_2$Mo$_2$O$_9$.

From Fig. 2, we find that each Mo cation is surrounded by four or five O ions, resulting in two MoO$_4$ tetrahedra, two MoO$_5$ hexahedra, three LaO$_8$ polyhedra, and one LaO$_7$ polyhedron in every final configuration. The O ions are thought to locate O(1)/O(2)/O(3) sites if they are closer to the crystallographic O(1)/O(2)/O(3) positions than other O sites, as shown in Fig. 3. We find that, within the maximum deviation smaller than 0.012 Å in x, y, or z axes, 12 final configura-
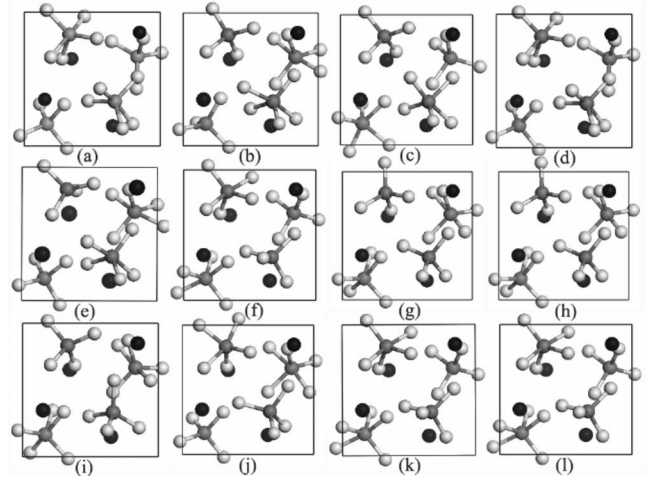

FIG. 2. Twelve final configurations of the 26-atom supercell quenched from 900 to 0 K. The O, Mo, and La ions are marked in small light gray, gray, and dark balls, respectively.

tions are connected to each other by one of 12 point operations of $P2_13$ space group. For example, the configuration shown in Fig. 2(a) is related to that shown in Fig. 2(b) by the operation $(xyz\rightarrow -z+1/2,-x,y+1/2)$ and associated with that shown in Fig. 2(e) by the operation $(xyz\rightarrow x+1/2,-y+1/2,-z)$ and with that shown in Fig. 2(i) by the operation $(xyz\rightarrow -x+1/2,-y,z+1/2)$. So these configurations are of symmetry of $P2_13$ space group and correspond to local structures (O ion arrangements) of β-La$_2$Mo$_2$O$_9$ and should thus represent the structural features of β-La$_2$Mo$_2$O$_9$. Each configuration has 18 O ions, giving 216 O ions in 12 final configurations. Of 216 O ions, 48 O ions are at O(1) sites, 132 O ions at O(2) sites, and 36 O ions at O(3) sites, resulting in 100%, 91.7%, and 25% occupancies of three crystallographic distinct O(1), O(2), and O(3) sites, respectively. The experimentally obtained occupancies are 100%, 87%, and 29% for O(1), O(2), and O(3) sites, respectively.[9] The theoretically calculated occupancy of O(2) sites is a little larger than the experimentally suggested, while the theoretical value of O(3) is a little smaller than the experimental. Cal-
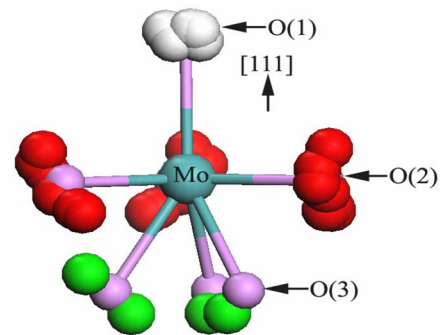

FIG. 3. (Color online) Statistical results of O ion arrangements around a Mo cation to distinguish O(1), O(2), and O(3) sites. The O(1), O(2), and O(3) atoms are marked in white, red (dark gray), and green (gray) balls, respectively. Three crystallographic distinct O ion sites are denoted by purple (light gray) balls.

TABLE I. Calculated Mo-O distances (Å) in MoO$_4$ and MoO$_5$ polyhedra. The data listed in the same column denote that the MoO$_4$ or MoO$_5$ polyhedra among the 12 final configurations are similar and the statistical uncertainties are less than 0.003 Å. The occupancies of three crystallographic distinct O(1), O(2), and O(3) sites are 100%, 91.7($\pm$8)%, and 25($\pm$8)%, respectively.

	MoO$_4$		MoO$_5$	
Mo-O(1)	1.809	1.794	1.952	1.943
Mo-O(2)	1.764	1.751	1.813	1.801
Mo-O(2)	1.765	1.779	1.833	1.803
Mo-O(2)	1.766		1.896	1.931
Mo-O(3)		1.773	1.829	1.882

culated Mo-O distances in MoO$_4$ tetrahedra and MoO$_5$ hexahedra are summarized in Table I. It should be stressed that the data listed in Table I are obtained by comparing the similar MoO$_4$ tetrahedra/MoO$_5$ hexahedra among the 12 final configurations, and the statistical uncertainties are small, less than 0.003 Å. The average values of Mo-O(1), Mo-O(2), and Mo-O(3) distances are 1.875, 1.809, and 1.828 Å, respectively, close to the corresponding experimental values of 1.821, 1.761, and 1.766 Å.[8] Mo-O(1) bond length is 0.15 Å shorter in MoO$_4$ tetrahedra than in MoO$_5$ hexahedra, which may be helpful for understanding the split of O(1) sites into two different groups suggested by NMR spectrum.[9] It should be pointed out that our present simulated supercells are small because it is time consuming. From the above comparison of the calculated and experimental atomic structures, our present simulated results are acceptable.

The average structure observed experimentally at any temperature must instead be interpreted as a time and spatial average of the different local structures which are energetically accessible at that temperature.[6,7] The different possible local structural configurations (in our present case, i.e., different O ion arrangements in available crystallographic sites) are assumed to correspond to separate local minima on the potential energy hypersurface of the system. Using this simple landscape analogy, the local or inherent structural configurations associated with the thermally accessible local energy minima are important not only for the average structure but also central when considering mechanisms for ionic transport. The heights of the saddle points separating the energy minima suggest energetically favorable transition paths between the different configurations and thus the mechanism of ionic transport and are helpful for us to understand the relaxation peaks in the mechanical and dielectric measurement. Such transition paths can be obtained theoretically using the NEB method. Three such minimum-energy transition paths are presented in Figs. 4(a)–4(c).

We find extremely low energy barrier 0.12 eV for the transition path between two configurations shown in Fig. 4(a). One O ion easily moves inside a MoO polyhedron from O(2) to O(3) site and simultaneously another O ions moves inside another MoO polyhedron from O(3) to O(2) site, or vice versa. Thus, in this case, O(2) and O(3) ions are highly active and move in concerted way, but does not diffuse along the MoO-polyhedron network, which can hardly contribute to the conductivity. At the saddle point, the bond length between moving O ion and its neighboring Mo cation is about 1.73 Å, indicating no MoO bond breaking.

As shown in Fig. 4(b), one O(2) ion moves to the unoccupied nearest-neighboring O(3) site in *another* MoO polyhedron [here, for convenience this motion process is simply marked with O(2)anotherO(3)] and simultaneously one O(3) ion jumps to the unoccupied nearest-neighboring O(2) site inside the *same* MoO polyhedron [O(3)sameO(2)]. The migration distance of O ion is 1.81 Å in O(2)anotherO(3) and 1.18 Å in O(3)sameO(2). At the transition state, MoO bond length is 2.48 Å in the O(2)anotherO(3) process and 1.74 Å in the O(3)sameO(2) process, indicating that only in O(2)anotherO(3) the MoO bond is broken. During this two-ion concerted diffusion process the energy barrier is 0.50 eV.

As shown in Fig. 4(c), the diffusion path involves the collective motion of O(1) and O(2) and O(3) ions. Using the similar mark, we can denote the collective diffusion process in Fig. 4(c) by three subprocesses: O(3)anotherO(1), O(1)sameO(2), and O(2)sameO(3). Note that here two referred O(1) sites are the same site and this site is occupied both in the initial and final states but by different O ions. The migration distance of O ion is 2.73 Å in O(3)anotherO(1) subprocess, 2.37 Å in O(1)sameO(2), and 1.08 Å in O(2)sameO(3). At the saddle point, MoO bond length is 2.13 Å in the O(3)anotherO(1) subprocess while is about 1.8 Å in other two subprocesses, implying that only one MoO bond is broken. The energy barrier is 1.24 eV in this three-ion collective motion process. Two subprocesses O(3)anotherO(1) and O(1)sameO(2) give an equivalent process O(3)anotherO(2) with the migration distance of 3.96 Å.
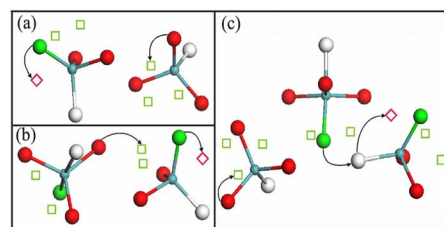

FIG. 4. (Color online) Schematic diagram of typical minimum-energy transition paths connecting the local structures. The O(1), O(2), O(3) and Mo atoms are marked in white, red (dark gray), green (gray), and small cyan (small gray) balls, respectively, and the unoccupied positions of O(2) and O(3) sites are marked in red (dark gray) and green (gray) squares, respectively. The arrows are guides to the eyes, and the start and end points of the arrow denote initial and final positions of the migration path, respectively.

It should be noted that this energy barrier is close to the experimental results, 0.9 and 1.1 eV in the mechanical relaxation measurement, 0.99 eV in the dielectric experiment, and 1.2 eV in the conductivity measurement.[1,4] This tells us that the collective diffusion of O(1) and O(2) and O(3) ions shown in Fig. 4(c) may be responsible for the mechanical and dielectric relaxation peaks. Though O(1) sites are fully occupied and O(2) and O(3) are partially occupied, O(1) ions are mobile such as O(2) and O(3) ions.

Diffusion can be supposed to proceed by a series of migration events. It is reasonable to calculate the diffusivity (D) by the product of the migration frequency (ν) and the migration length (λ), $D = \nu\lambda$. The migration frequency is usually sensitive to the concentration of movable ions and should exponentially depend on the barrier energy as a function of $-\frac{E_b}{T}$. In two-ion migration event, E_b is equal to 0.5 eV and λ is about 2 Å, while in three-ion migration event, E_b is equal to 1.24 eV and λ is close to 4 Å. Both events involve the concerted motions O(2) and O(3), indicating no difference in the concentration dependence of ν between these two events. Thus, both two-ion and three-ion migration events are responsible for the high conductivity of β-La$_2$Mo$_2$O$_9$.

These results not only show the concerted transport of O(1), O(2), and O(3) ions instead of the single-jump mechanism but also clearly elucidate their contribution to the ionic conductivity in β-La$_2$Mo$_2$O$_9$. It is important to stress that we could not find the diffusion path involving only one O ions, for example, O(2)another/sameO(3). That is, the mobile ions move in a cooperative fashion. Although the motion of O ions is thermally activated, the cooperativity gives rise to the phenomenon that could not be understood by the independent single-particle jump. For example, as mentioned in the Introduction, the height of internal friction peak observed in the mechanical relaxation measurement hardly changes with temperature and the relationship between the conductivity and temperature follows VTF equation. Though O(1), O(2), and O(3) ions move in collective way, only one O ion plays a leading role in the energy barrier and the migration distance. In other words, the migration of one O ion from one MoO polyhedron to another must be simultaneously assisted by the motion of another O ions. As we know, Arrhenius and VTF models are prototypes for activated and assisted transport mechanisms, respectively. Thus, the diffusion behavior in β-La$_2$Mo$_2$O$_9$ could be analyzed using the combined model of Arrhenius and VTF. The collective ionic motion suggested here bears similarities to recent reports of quasicollective surface diffusion involving several atoms for metal surfaces by transmission electron microscopy[21] and by density-functional theory NEB calculations,[22] and collective ionic motion in oxygen-deficient perovskites such as oxide fast ion conductor Ba$_2$In$_2$O$_5$.[6,7]

IV. CONCLUSION

In summary, by *ab initio* MD simulations coupled to a simulated annealing procedure and the nudged elastic band method, we have revealed the structure features of β-La$_2$Mo$_2$O$_9$ and the multi-ion concerted migration in β-La$_2$Mo$_2$O$_9$. Each Mo cation is surrounded by four or five O ions. O(1) sites are fully occupied, and O(2) and O(3) are partially occupied. The data of Mo-O(1) bond length show the split of O(1) sites into two different groups. O(1) ions are mobile such as O(2) and O(3) ions. The mobile ions move in a cooperative fashion. Two diffusion channels are found to be responsible for the high conductivity, one involves the migration of O(2) ion with low activation energy and short migration length assisted by O(3), and another is the migration of O(3) with large activation energy and long migration length assisted by O(1) and O(2) ions. Thus, the diffusion or relaxation behavior in β-La$_2$Mo$_2$O$_9$ could be understood using the combined model of Arrhenius and VTF. Although the small cell size to which we are restricted by the *ab initio* MD method, the cell size does not affect our interpretation of the general features of the transition pathways that leads to the converted oxygen-ion motion. It should be attractive and fruitful to suggest that this type of collective ionic motion is a characteristic of fast ionic conductors with different kinds of occupied and/or unoccupied sites in general and also may be helpful to study the collective transport behavior in other disorder materials.

*Author to whom correspondence should be addressed; csliu@issp.ac.cn

[1] P. Lacorre, F. Goutenoire, O. Bohnke, and R. Retoux, Nature (London) **404**, 856 (2000).

[2] S. Georges, F. Goutenoir, O. Bohnke, M. C. Steil, S. J. Skinner, H-D Wiemhofer, and P. Lacorre, J. New Mater. Electrochem. Syst. **7**, 51 (2004).

[3] P. Lacorre, A. Selmi, G. Corbel, and B. Boulard, Inorg. Chem. **45**, 627 (2006).

[4] X. P. Wang and Q. F. Fang, Phys. Rev. B **65**, 064304 (2002).

[5] X. P. Wang, D. Li, Q. F. Fang, Z. J. Cheng, G. Corbel, and P. Lacorre, Appl. Phys. Lett. **89**, 021904 (2006).

[6] S. Stolen, E. Bakken, and C. E. Mohn, Phys. Chem. Chem. Phys. **8**, 429 (2006).

[7] C. E. Mohn, N. L. Allan, C. L. Freeman, P. Ravindran, and S. Stolen, Phys. Chem. Chem. Phys. **6**, 3052 (2004).

[8] F. Goutenoire, O. Isnard, and P. Lacorre, Chem. Mater. **12**, 2575 (2000).

[9] G. Corbel, Y. Laligant, F. Goutenoire, E. Suard, and P. Lacorre, Chem. Mater. **17**, 4678 (2005).

[10] P. Lacorre, Solid State Sci. **2**, 755 (2000).

[11] J. Emery, D. Massiot, P. Lacorre, Y. Laligant, and K. Conder, Magn. Reson. Chem. **43**, 366 (2005).

[12] P. E. Blochl, Phys. Rev. B **50**, 17953 (1994).

[13] G. Kresse and D. Joubert, Phys. Rev. B **59**, 1758 (1999).

[14] G. Kresse and J. Furthmuller, Phys. Rev. B **54**, 11169 (1996).

[15] H. J. Monkhorst and J. D. Pack, Phys. Rev. B **13**, 5188 (1976).

[16] F. H. Stillinger and T. A. Weber, Phys. Rev. A **25**, 978 (1982); **28**, 2408 (1983).

[17] C. S. Liu, Z. G. Zhu, J. C. Xia, and D. Y. Sun, Phys. Rev. B **60**, 3194 (1999); Z. G. Zhu and C. S. Liu, *ibid.* **61**, 9322 (2000).

[18] G. Henkelman, B. P. Uberuaga, and H. Jónsson, J. Chem. Phys. **113**, 9901 (2000); G. Henkelman and H. Jónsson, *ibid.* **113**, 9978 (2000).

[19] F. A. Lindemann, Phys. Z. **11**, 609 (1910).

[20] D. Y. Sun and X. G. Gong, Phys. Rev. B **57**, 4730 (1998).

[21] M. Labayen, C. Ramirez, W. Schattke, and O. M. Magnussen, Nat. Mater. **2**, 783 (2003).

[22] G. Henkelman and H. Jónsson, Phys. Rev. Lett. **90**, 116101 (2003).